Supplementary Information Appendix

Supplementary Materials and Methods

Construct design

Fifteen clade C *env* genes were assessed by various parameters that appear to correlate with native-like trimer structure and/or antigenicity. For all sequences, we introduced the following changes to create SOSIP.664 gp140 constructs, as previously described: A501C and T605C (gp120-gp41$_{ECTO}$ disulfide bond (1)); I559P in gp41$_{ecto}$ (trimer-stabilizing (2)); REKR to RRRRRR in gp120 (enhancement in cleavage efficiency (3)); TPA leader peptide (increase in gene expression (4)); and stop codon after gp41$_{ecto}$ residue 664 (improvement of solubility and homogeneity (5, 6)). Finally, we introduced canonical *N*-linked glycosylation sites at positions 156, 160, 295, 301, 332, 386, 392 or 448, if absent from the wild-type sequences, to restore or improve the epitopes for various bnAbs with glycan-dependent epitopes. For example, K295N and D386N substitutions were introduced into the DU422 sequence, and D156N, E295N, V297T and D332N changes into the ZM197M sequence. Similarly, and for the same reason, the BG505 SOSIP.664 trimers contain a T332N substitution (7). The resulting, codon-optimized clade C SOSIP.664 *env* genes were synthesized at Genscript (Piscataway, NJ) and cloned into pPPI4 using *PstI* and *NotI* restriction sites (1). For ELISA and SPR studies, we made trimers containing a D7324 epitope-tag sequence at the C-terminus of gp41 by adding the amino-acid sequence GSAPTKAKRRVVQREKR after residue 664 in gp41, as previously described (7). The resulting trimers are designated SOSIP.664-D7324.

Screening of Env protein expression by transient transfection

In initial studies, SOSIP.664 proteins were expressed in a suspension HEK 293 cell line that is deficient in the glycosyl transferase I enzyme, termed GnT I$^{-/-}$ and referred to hereafter as 293S cells, by transient transfection of *env* genes using 293Fectin (Invitrogen) as previously described (8). Env proteins produced in 293S cells contain unprocessed, high mannose glycoforms. All SOSIP.664 trimer-encoding *env* genes were co-transfected with the *furin* gene to maximize trimer cleavage (1). In each preparation, 500 mL of cells were transfected at a density of 0.5-0.8 x 10^6 cells/mL and harvested after 6-7 days. Suspension cultures were centrifuged at 6,000 x g

for 30 min and the supernatant was passed through a 0.22 μm filter, prior to loading on a column containing 25 mL *Galanthus nivalis* Lectin (GNL) resin (Vector Labs). Env proteins were eluted with 1x phosphate-buffered saline (PBS) containing 1 M methyl α-D-mannopyranoside after the column had been washed with 1x PBS containing 0.5 M sodium chloride. The eluted sample was diluted in PBS and concentrated to 0.5 mL using a 30K MWCO Amicon Ultra-15 Centrifugal filter unit (EMD-Millipore) prior to loading on a Superose 6 10/300 GL SEC column (GE Healthcare). The trimer yields (%) were calculated as follows: amount of trimer recovered from the SEC column divided by the amount of GNL-purified Env protein loaded onto the column. To consistently define the SEC trimer peak, we used areas on both side of the apex at ~25% of the peak height.

In follow-up experiments, to prepare SOSIP.664 trimers for ITC, SEC, ELISA, SPR and cryo-EM studies, selected proteins were produced in wild-type suspension HEK 293F cells (hereafter referred to as 293F cells) using the identical transfection protocol described above. SOSIP.664 trimers produced in 293F cells have a wild-type glycosylation profile and are more suitable for antigenicity studies. For additional ELISA-based antigenicity and cryo-EM studies, we also purified selected SOSIP.664 proteins via a PGT145-affinity or 2G12-affinity column with $MgCl_2$ elution followed by SEC to isolate trimers, as previously described (7, 9, 10).

Negative stain electron microscopy (NS-EM)

The DU422 and ZM197M SOSIP.664 trimers were prepared for NS-EM analysis as previously described (7, 9, 10). Using concentrations determined by A280 with theoretical extinction coefficients derived from the primary sequence of the proteins (11), trimer samples were diluted to between 0.01-0.5 mg/mL in Tris-buffered saline (TBS), pH 7.4 and adhered onto a carbon-coated 400 Cu mesh grid that had been glow discharged at 15 mA for 30 s by applying a 3 μL drop for 5-10 s followed by blotting with filter paper. Grids were then stained with 2% (w/v) uranyl formate for 60 s. Data were collected using an FEI Tecnai T12 electron microscope operating at 120 keV, with an electron dose of ~25 $e^-/Å^2$ and a magnification of 52,000x that resulted in a pixel size of 2.05 Å at the specimen plane. Images were acquired with a Tietz TemCam-F416 CMOS camera using a nominal defocus of 1,000 nm.

Data processing methods were based on those previously reported (10). Briefly, particles were picked automatically using DoG Picker and put into a particle stack using the Appion

software package (12, 13). Initial, reference-free, two-dimensional (2D) class averages were calculated using particles binned by two via iterative Multivariate Statistical Analysis (MSA)/Multi-reference Alignment (MRA) and sorted into classes (14). In general, the number of classes requested was enough to result in an average of 50 particles per class. Particles that corresponded to stain artifacts or noise (uniform gray squares) were discarded from future analyses. Additionally, the number of particles not corresponding to the mass of a trimer (e.g. dimers, monomers, aggregates, and contaminating proteins) were recorded for the purpose of assessing trimer purity but also removed from subsequent alignments. The remaining particles were placed into a sub-stack and binned by two before another round of reference-free alignment was carried out using iterative MSA/MRA (14). The final round of 2D class averages were visually inspected and segregated into one of three trimer structural groups designated as "closed", "partially open" or "non-native", as previously described (10). Briefly, to allow greater discernibility between the “partially open vs closed” averaged particles, classification of at least 5,000 particles was performed using reference datasets that average 50 particles per class, and such datasets often contained 200-300 class averages that meet this criterion.

Differential scanning calorimetry (DSC)

Thermal denaturation was probed with a MicroCal VP-Capillary calorimeter (GE Healthcare) (7). 293S cell-produced SOSIP.664 trimers purified by the GNL/SEC method were extensively dialyzed against PBS. The trimers were subsequently adjusted to a concentration of approximately 0.1 - 0.3 mg/mL (0.5 - 1 μM) before loading into the cell. Thermal denaturation was probed at a scan rate of 90° C/h. Buffer correction, normalization and baseline subtraction procedures were manually inspected before the data were automatically analyzed using a standardized protocol from the Origin 7.0 software.

Antibodies and Fabs

The PGT145 and VRC01 Fabs were expressed and purified via an anti-human κ light chain affinity matrix (CaptureSelect Fab κ; BAC), followed by cation-exchange chromatography, as previously described (15-17). MAb 19b was expressed in 293F cells from plasmids kindly provided by James Robinson and purified via Protein A or G affinity chromatography using the manufacturer’s recommended protocol (GE Healthcare). MAbs used in ELISA and

neutralization assays were obtained as gifts, purchased, or expressed from plasmids from the following sources: John Mascola and Peter Kwong (VRC01, VRC26.09); International AIDS Vaccine Initiative (PG16, PGT121, PGT145, PGT151, b6); Polymun Scientific (2G12); Michel Nussenzweig (3BC315); James Robinson (17b, 14e); and Mark Connors (35O22).

Isothermal titration calorimetry (ITC)

ITC binding experiments were performed using an Auto-iTC200 instrument (GE Healthcare), as previously described (8, 18). Briefly, proteins were first dialyzed against TBS. Subsequently, using UV absorbance at 280 nm with calculated extinction coefficients from the primary amino-acid sequence (11), protein concentrations were adjusted to 10 - 100 μM for the 19b IgG present in the syringe, and to 3 - 5 μM for the SOSIP.664 trimers present in the cell. For each binding experiment, the reference power was 5 μcal. The first injection was 0.5 μL, and was followed by 15 injections of 2.5 μl each at intervals of 180 s. We used Origin 7.0 software to fit the integrated titration peaks via a single-site binding model and derive the stoichiometry of binding (N), the affinity constant (K_d) and the molar reaction enthalpy (ΔH). All measured and derived thermodynamic parameters of binding are reported in Table S1.

D7324-capture ELISA

ELISAs using GNL/SEC- or 2G12/SEC-purified SOSIP.664-D7324 trimers produced in 293F cells were performed essentially as described previously (7, 9). The input trimer concentration was 300 ng/mL. The sheep polyclonal Ab D7324 to a gp120 C5-epitope used for coating the ELISA wells was obtained from Aalto Bioreagents, Dublin, Ireland.

Surface Plasmon Resonance (SPR)

SPR was performed as described previously (19). Briefly, the D7324 Ab was covalently immobilized to ~15,000 response units (RU) to CM5 chips. D7324-epitope-tagged SOSIP trimers were then captured (~500 RU). The test MAbs were then injected at a concentration of 500 nM and flow rate of 50 μL/min. After each cycle of MAb association (300s) and dissociation (600s), the D7324 surface was regenerated by a single injection of 10 mM glycine (pH 1.5) for 60 s at a flow rate of 30 μL/min.

Neutralization assays

To determine the extent of HIV-1 neutralization by MAbs, we used Env-pseudotyped viruses and a single cycle infection assay based on TZM-bl cells, as described previously (7). All infections were performed in duplicate. Uninfected cells were used to correct for background luciferase activity. The infectivity of each mutant without inhibitor was set at 100%. Nonlinear regression curves were determined and 50% inhibitory concentrations (IC_{50}) were calculated using a sigmoid function in Prism software version 5.0. Drs. Celia LaBranche and David Montefiori (Duke University Central Laboratory, Durham, NC) have classified the wild type DU422 and ZM197M Env-pseudotyped viruses as having tier-2 and tier-1B neutralization sensitivity, respectively, and their glycan-modified variants (herein termed DU422* and ZM197M*) have unchanged properties (20-22). A Spearman correlation analysis of the ELISA-derived antigenicity *vs.* neutralization data was performed in Prism software version 6.0, as previously described (7, 10).

Cryo-electron microscopy

The VRC01 Fab + ZM197M SOSIP.664 complex was generated by adding a 6-fold molar excess of VRC01 Fab to the trimer, and incubating the mixture at room temperature for ~1 h. Excess Fab was removed by purification over a Superose 6 column (GE Healthcare). Fab + trimer complex fractions were pooled and concentrated to ~1.5 mg/mL. n-dodecyl β-D-maltopyranoside (DDM) was added to the sample just prior to freezing such that its final concentration in the solution was ~0.018%. A 3 μL aliquot of the sample was applied to 2/2 C-Flat holey grids, and blotted at room temperature, and the grids were then immediately plunged into liquid ethane. Data were collected using our Titan Krios electron microscope operating at 300 kV, equipped with a Gatan K2 direct electron detector camera using the Leginon interface (23). Exposure images were collected in counting mode at 25,500x magnification resulting in a pixel size of 1.31 Å on the specimen plane. With a 200 msec exposure per frame, the total exposure dose was ~31.6 $e^-/Å^2$. Images were shot at a random nominal defoci range between -2.00 and -3.20 μm. All frames were aligned for use in processing (24). CTF estimation was performed using CTFFind3 (25). Particles were automatically selected using DoG Picker (12, 13), boxed out using a box size of 256x256 pixels, and sorted by a single round of reference-free 2D class averaging using MRA/MSA (14). The 2D sorted particles were further sorted by 2 rounds of 3D

classification using particles binned by 4, without imposing symmetry, and using an unliganded trimer structure (EMD-5782) (26) low-pass filtered to 60 Å as an initial model in Relion (27). The 4,903 particles belonging to the best 3D class were used for an unbinned refinement. The final refinement was performed using the Relion auto-refine function, with internal CTF correction (27). The model resolution was determined to be 9.58 Å by a gold-standard Fourier shell correlation curve using a correlation cut-off of 0.143, following the application of a soft edge mask as outlined in Chen *et al.* (28). A B-factor of -609 $Å^2$, which was determined by the program using the MTF of the K2 camera at 300 kV (27), was applied to obtain the final sharpened reconstruction and to enhance the higher resolution contributions.

Supplementary Figures

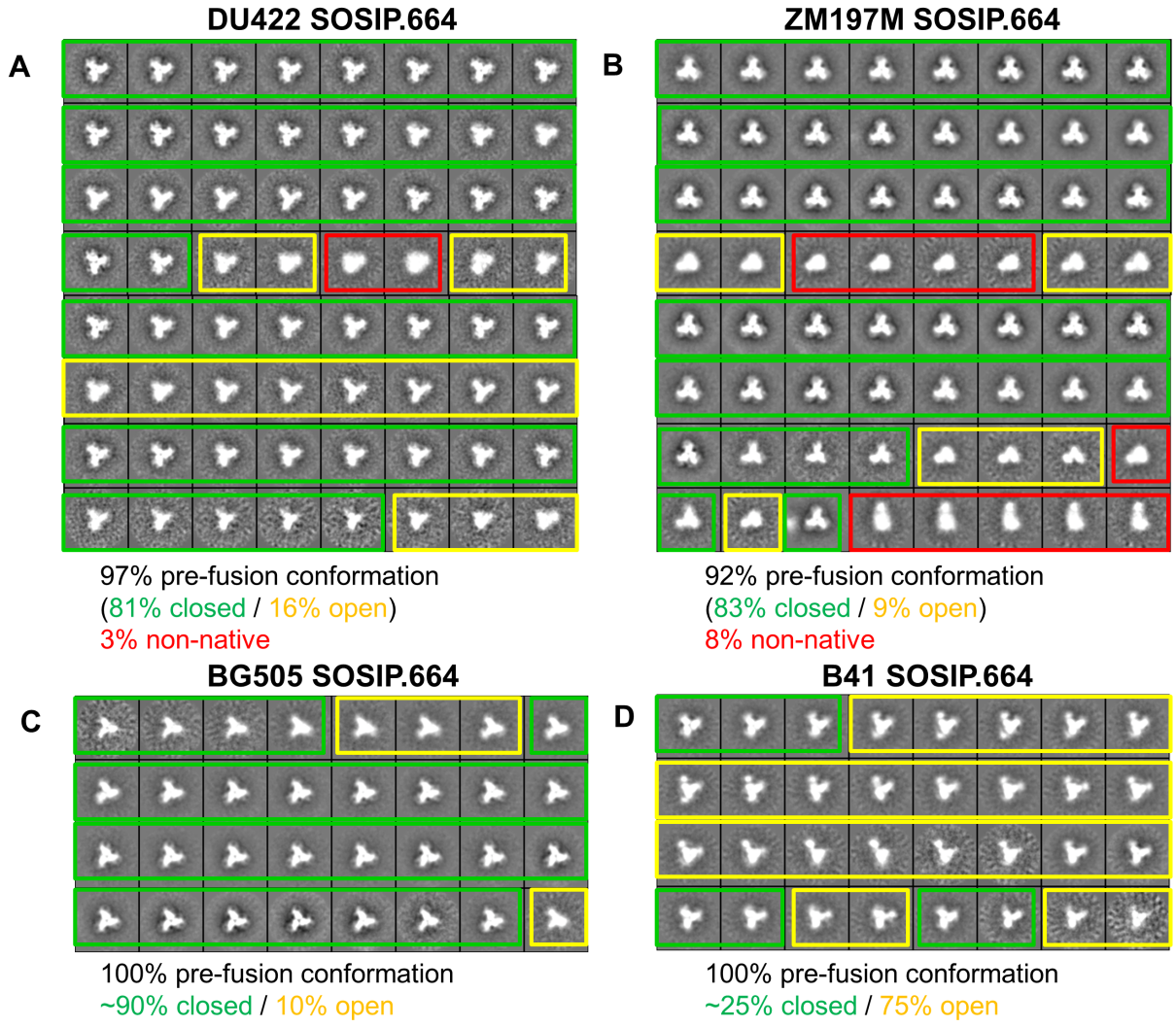

Figure S1. Two-dimensional negative-stain electron microscopy class averages of *(A)* DU422, *(B)* ZM197M, *(C)* BG505 and *(D)* B41 SOSIP.664 trimers. Classes representing native-like trimers in a closed, compact state similar to those typically seen with BG505 SOSIP.664 trimers are outlined in green. Classes that represent more open, but still native-like trimers, as evidenced by the appearance of additional density without loss of apparent mass of the trimer and/or blurring of the trimer, are outlined in yellow. Env proteins lacking any clear trimeric morphology are highlighted in red. Percentage classifications were calculated by dividing the total number of trimeric particles in each sub-category by the total number of trimeric particles.

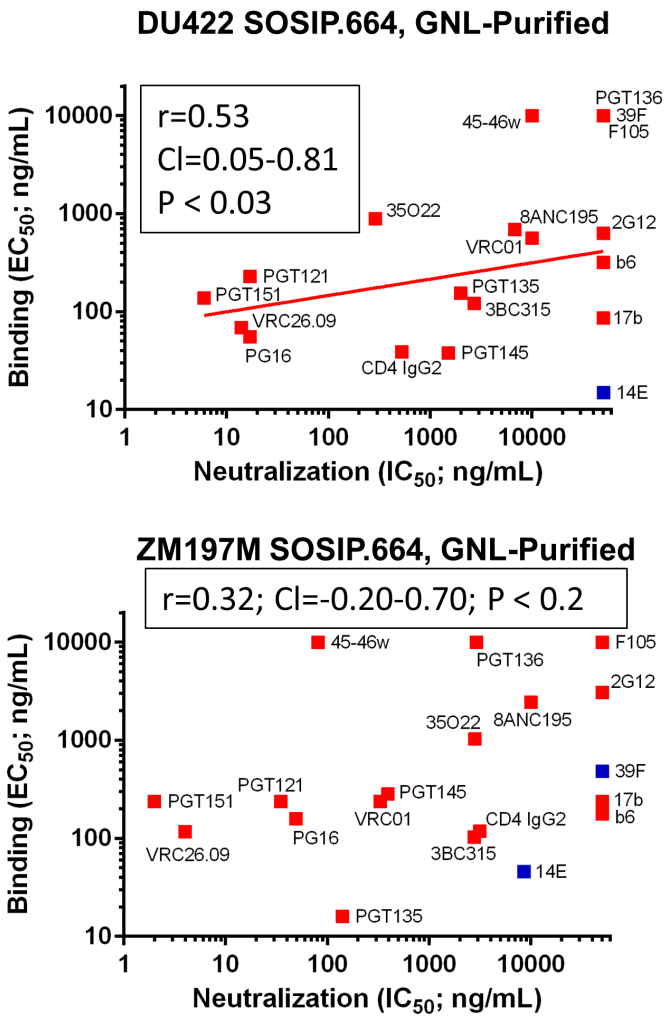

Figure S2. GNL-affinity purification produces a lower proportion of antigenically native DU422 and ZM197M SOSIP.664 trimers, compared to 2G12-affinity purification. The ELISA-derived antigenicity *vs.* Env-pseudovirus neutralization analysis generates much weaker Spearman correlations (inset), especially for ZM197M, when the trimers are purified by GNL/SEC rather than by 2G12/SEC (Fig. 3). bnAbs and non-nAbs were selected to represent an array of epitopes. Data points colored red were included in the correlation analysis, and colored blue if omitted. The V3 non-nAbs 14E and 39F were excluded from the correlation analysis, as immobilization of SOSIP.664-D7324 trimers on ELISA plates exacerbates the exposure of V3 epitopes in a way not reflected by other techniques (7). No fit was drawn through the data in the ZM197M graph because the correlation was not significant ($p>0.05$).

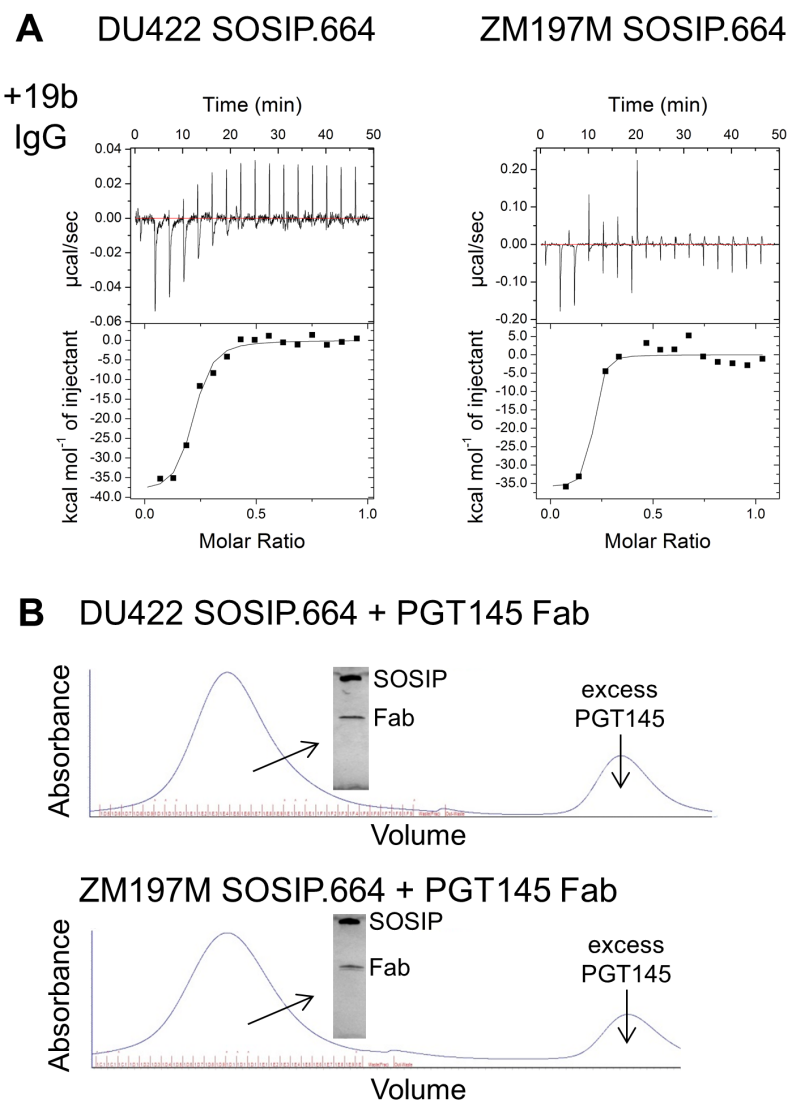

Figure S3. Weak binding of a non-neutralizing V3-reactive antibody and strong binding of a quaternary-specific bNAb to clade C SOSIP.664 trimers purified by GNL/SEC. *(A)* Binding of DU422 and ZM197M trimers produced in 293F cells to the 19b IgG non-NAb, as measured by ITC. The top panels show the raw data, and the bottom the binding isotherms derived from the integrated heat of binding, for representative experiments. A weak signal indicative of low stoichiometry is observed for 19b binding. The measured and derived thermodynamic parameters of binding are reported in Table S1. *(B)* SEC was performed on the SOSIP.664 trimers after incubation with an excess of PGT145 Fab. A stable antigen-antibody complex was isolated by SEC, as demonstrated by SDS-PAGE electrophoresis (inset).

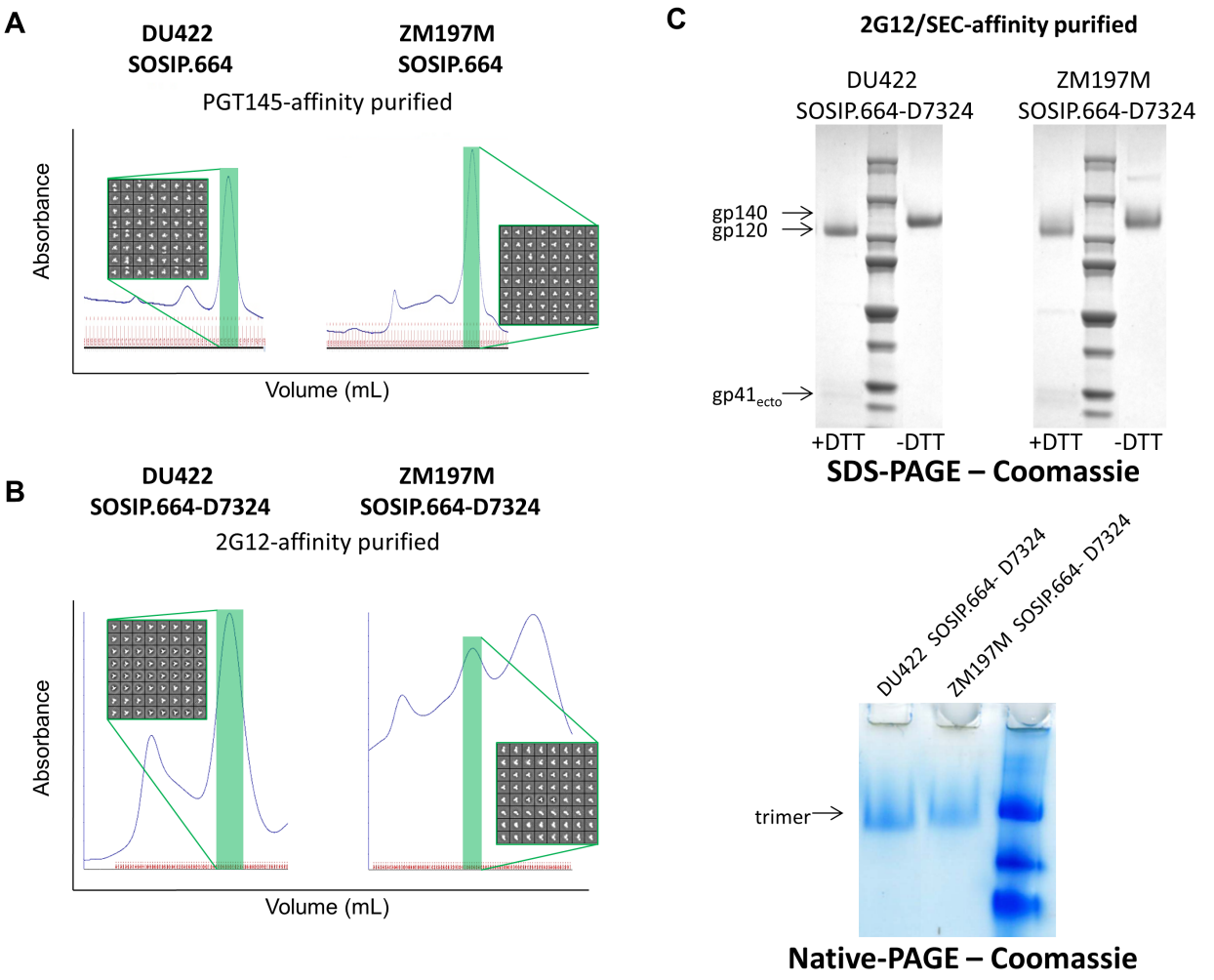

Figure S4. Positive-selection affinity purification of DU422 and ZM197M SOSIP.664 trimers. SEC profiles are shown for *(A)* PGT145- and *(B)* 2G12-affinity purified DU422 and ZM197M SOSIP.664 constructs, with the shaded green area indicative of trimers. NS-EM analyses (inset, showing representative 2D-class averages of the trimers) reveal that these trimers predominantly adopt a pre-fusion conformation when purified by either method. *(C)* SDS-PAGE and Blue Native-PAGE analysis show efficient gp120-gp41 cleavage (dissociation of gp140 into gp120 and gp41 subunits in SDS-PAGE upon addition of DTT) and high purity, respectively for the DU422 and ZM197M SOSIP.664-D7324 trimers purified by 2G12/SEC that were subsequently used as reagents in ELISA and SPR affinity measurements.

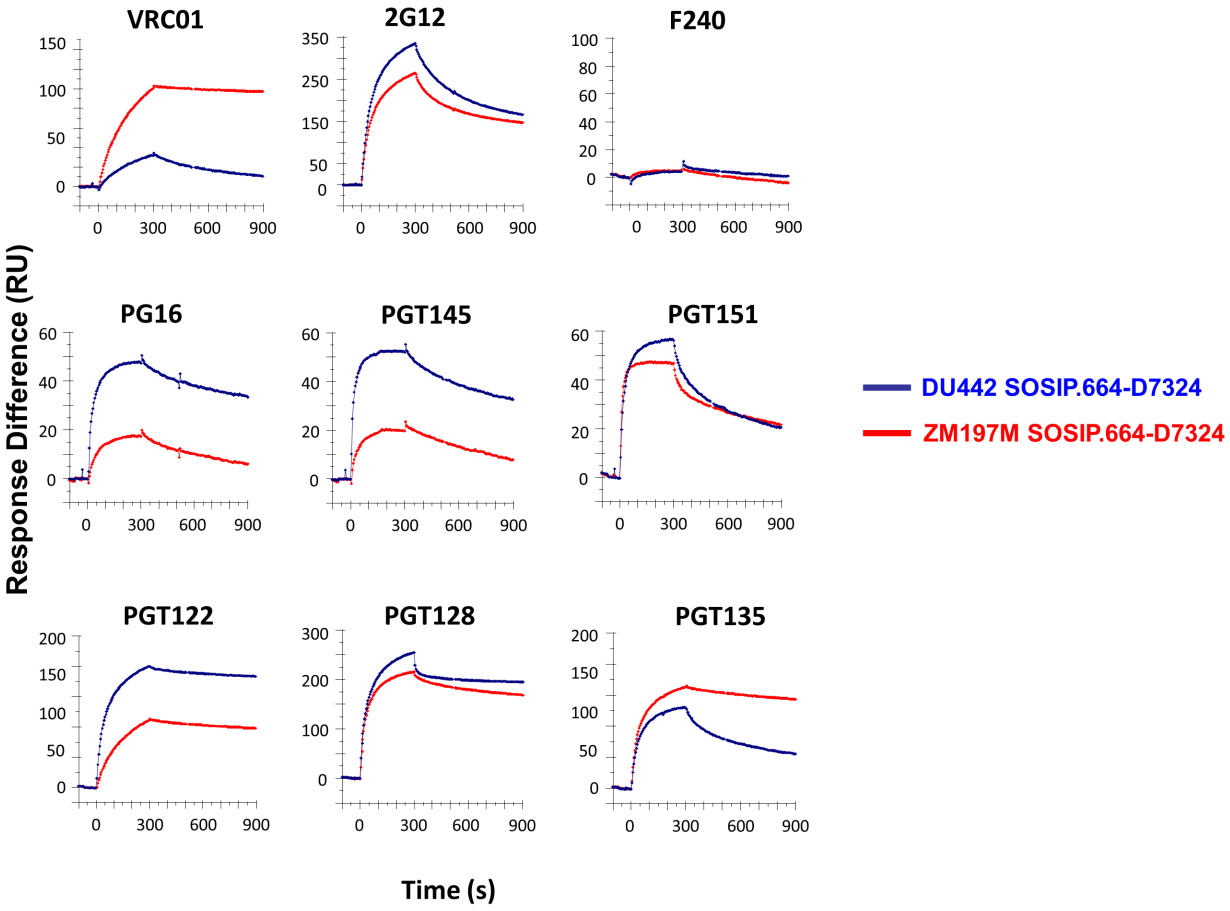

Figure S5. SPR binding measurements of various bnAbs to 2G12/SEC-purified, D7324-tagged DU422 and ZM197M SOSIP.664 trimers. Overall, SPR binding corroborates ELISA binding data, and correlates well with neutralization IC_{50} values for the corresponding Env-pseudotyped viruses (Table S2). For example, DU422 SOSIP.664 trimers are only weakly reactive with VRC01 and PGT135. These antibodies neutralize the DU422 Env-pseudotyped virus only weakly (Table S2). In contrast, the ZM197 SOSIP.664 trimers bind well to these two bnAbs, which neutralize this virus potently. The non-nAb F240 was used as a negative control.

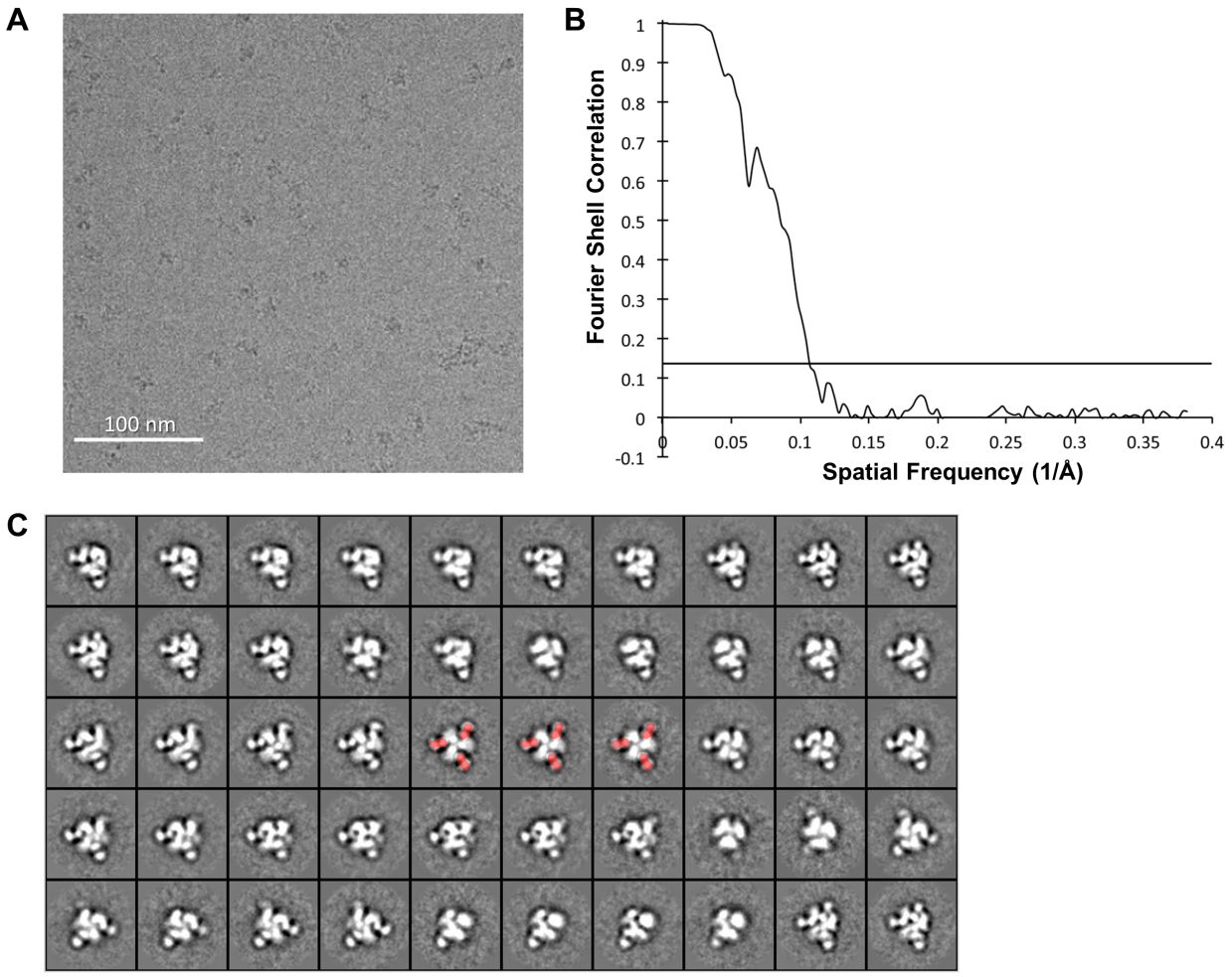

Figure S6. Cryo-electron microscopy of the ZM197M SOSIP.664 trimer + VRC01 Fab complex. *(A)* Frame aligned micrograph at 25,500x magnification, using a -2.80 μm defocus, and a dose rate of 31.6 e-/Å^2. *(B)* Gold-standard Fourier shell correlation (FSC) curve between two independent models generated during refinement. The final resolution of the B-factor corrected model at an FSC cut-off of 0.143 is 9.58 Å. *(C)* Reference-free 2D class averages of the particles that went into the final refinement are shown. In some class-averages, density attributed to the VRC01 Fab is colored in red for clarity.

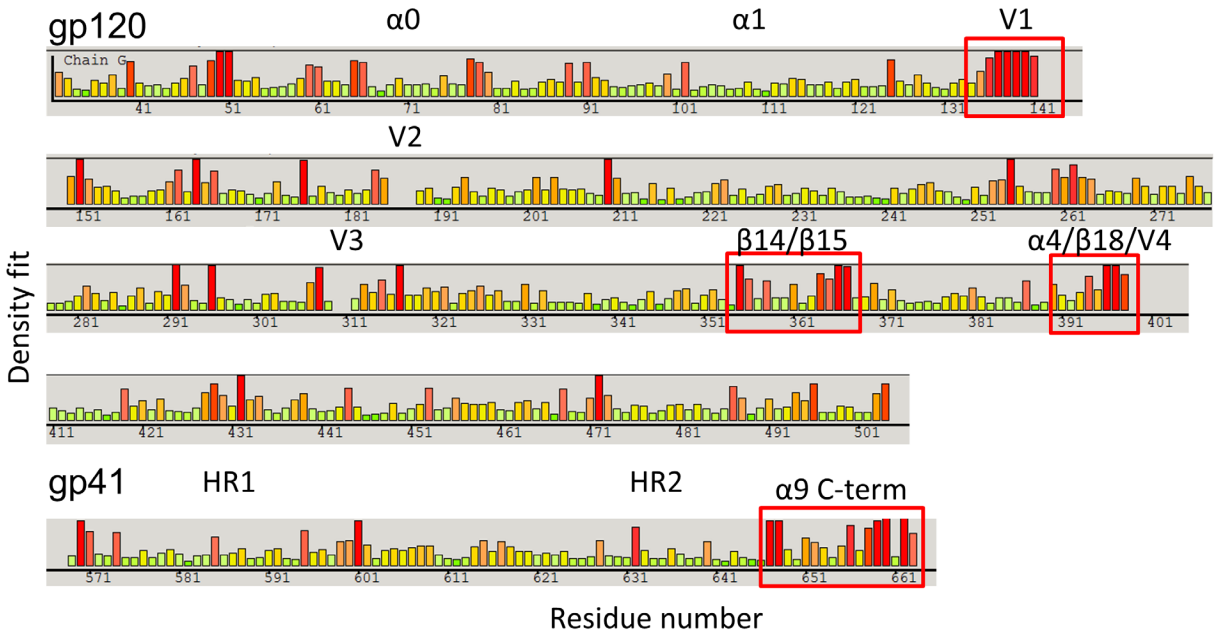

Figure S7. Density fit analysis of the 4.4 Å crystal structure of the BG505 SOSIP.664 trimer + NIH45/46 scFv complex into the 9.6 Å reconstruction of the ZM197M SOSIP.664 trimer + VRC01 Fab complex. Density fit is reported as a color-coded bar graph where lower values with greener colors represent a better fit to the density and higher values with redder colors indicate a poorer fit. Gaps indicate either a region not modeled in the structure (e.g. gp120 V2 and V4), or numbering differences between the BG505 sequence and the HXB2 reference (e.g. gp120 V1 and V3). The 9.6 Å resolution of the cryo-EM reconstruction does not allow a confident determination of the fit of individual residues, but consecutive stretches of poor density fit can confidently be assigned to structural elements that show a significant difference between the BG505 SOSIP.664 trimer + NIH45/46 scFv 4.4 Å crystal structure (PDB 5D9Q) and the ZM197M SOSIP.664 trimer + VRC01 Fab 9.6 Å reconstruction. Density fitting was performed using the "Density Fit Analysis" function in Coot (29).

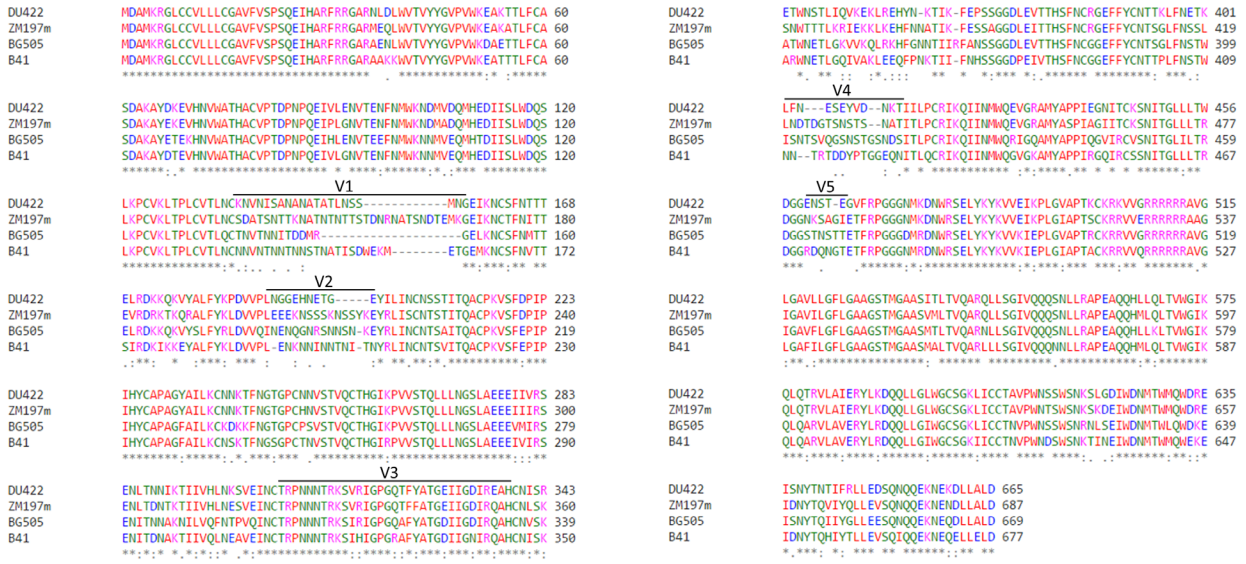

Figure S8. Alignment of the clade A BG505, clade B B41 and clade C DU422 and ZM197M SOSIP.664 amino-acid sequences. Sequence alignment was performed in the EMBL-EBI ClustalW2 web services for Multiple Sequence Alignment (30). Amino acids are colored by type, and the asterisk, colon and period symbols below the sequence denote amino acids with conserved, strongly similar and weakly similar properties, respectively, according to the EMBL-EBI ClustalW2 convention (30). The lack of any symbol indicates that different amino acids are present at the position.

Supplementary Tables

Table S1. Isothermal titration calorimetry (ITC) binding of 19b to the DU422 and ZM197M clade C SOSIP.664 trimers in comparison with BG505 (clade A) and B41 (clade B).

Epitope	Binding experiment[&]	ΔG_1[%] (kcal mol^{-1})	ΔH_1[%] (kcal mol^{-1})	$-T\Delta S_1$[%] (kcal mol^{-1})	K_{d1}[%] (nM)	N_1[%]
V3 tip, non-neut	[#]19b IgG into BG505 SOSIP.664	-10.6	-41.4	30.8	21	0.1
	[#]19b IgG into B41 SOSIP.664	-11.9	-39.5	27.6	3	0.2
	19b IgG into DU422 SOSIP.664	-10.3	-39.1	28.8	26	0.2
	19b IgG into ZM197 SOSIP SOSIP.664	-11.0	-36.1	25.1	10	0.2

[%]Reported values are averages from at least two independent measurements and associated errors are approximately 10% of the average. Representative isotherms can be found in SI appendix, Fig. S3.
[#]Reported in (10).
[&]All trimers were expressed in 293F cells. DU422 and ZM197 trimers were purified by GNL/SEC, whereas BG505 and B41 trimers were purified by 2G12/SEC.

Table S2. MAb binding to DU422 and ZM197M SOSIP.664-D7324 trimers as determined by ELISA and neutralization of the corresponding Env-pseudotyped viruses. Midpoint neutralization concentrations (IC_{50}, in ng/mL) and half-maximal binding concentrations (EC_{50}, in ng/mL) are compared with data derived using the BG505 and B41 SOSIP.664-D7324 trimers.

		Clade A BG505[#]		Clade B B41[&]		Clade C ZM197M		Clade C DU422	
Epitope	Antibody	IC_{50} (ng/mL)	EC_{50} (ng/mL)	IC_{50} (ng/mL)	EC_{50} (ng/mL)	IC_{50} (ng/mL)	EC_{50} (ng/mL)	IC_{50} (ng/mL)	EC_{50} (ng/mL)
V1/V2 glycan	PG9	45	343	560	490	393	weak	88	weak
	PG16	8	199	80	210	49	340	17	76
	PGT145	83	114	60	200	393	197	1,511	698
	VRC026	ND[%]	ND[%]	ND	ND	4	58	14	98
gp120-gp41 interface	PGT151	ND[%]	ND[%]	30	>20,000	2	24	6	29
	35O22	ND[%]	ND[%]	>50,000	>20,000	2,816	1,288	288	1,298
	8ANC195	139	2,065	1,890	5,680	>10,000	343	>10,000	649
Unknown	3BC315	1,259	962	ND	ND	3,549	127	2,690	152
CD4bs nAbs	CD4-IgG2	433	155	8,490	>20,000	2,763	109	529	152
	VRC01	70	163	1,380	1,040	329	237	6,767	200
	45-46W	23	67	ND	ND	81	669	>10,000	435
CD4bs non-nAbs	b6	>30,000	871	>50,000	>20,000	>50,000	907	>50,000	757
	F105	>30,000	>10,000	>50,000	>20,000	>50,000	>10,000	>50,000	>10,000
CD4i	17b	>30,000	>10,000	>50,000	>20,000	>50,000	3,709	>50,000	2,990
V3 glycan	PGT121	15	95	920	450	35	267	17	322
OD-glycan	2G12	790	27	12,780	220	>50,000	305	>50,000	117
	PGT135	2,234	521	20,300	4,830	140	676	1,985	481
	PGT136	25,667	434	ND	ND	2,911	>10,000	>50,000	>10,000
V3	14E	>30,000	28	>50,000	150	8,579	175	>50,000	58
	39F	>30,000	160	>50,000	40	>50,000	433	>50,000	3,726
$gp41_{ECTO}$, non-nAb	F240	>30,000	>10,000	>50,000	>20,000	ND	>10,000	ND	>10,000
Spearman correlation, R		0.88[$]		0.69[*]		0.71		0.77	

[#]Described in detail in (7).
[%] Values not determined in (7), but it is now known that BG505 SOSIP.664 trimers do bind these bNAbs (15, 31, 32).
[$]Previously reported in (7), with n=45.
[&]Described in detail in (10).
[*]Previously reported in (10), with n=19.
[&]All D7324-tagged trimers were expressed in 293F cells and purified by 2G12/SEC.

Supplementary References

1. Binley JM, *et al.* (2000) A recombinant human immunodeficiency virus type 1 envelope glycoprotein complex stabilized by an intermolecular disulfide bond between the gp120 and gp41 subunits is an antigenic mimic of the trimeric virion-associated structure. *J Virol* 74(2):627-643.
2. Sanders RW, *et al.* (2002) Stabilization of the soluble, cleaved, trimeric form of the envelope glycoprotein complex of human immunodeficiency virus type 1. *J Virol* 76(17):8875-8889.
3. Binley JM, *et al.* (2002) Enhancing the proteolytic maturation of human immunodeficiency virus type 1 envelope glycoproteins. *J Virol* 76(6):2606-2616.
4. Sellhorn G, Caldwell Z, Mineart C, & Stamatatos L (2009) Improving the expression of recombinant soluble HIV Envelope glycoproteins using pseudo-stable transient transfection. *Vaccine* 28(2):430-436.
5. Khayat R, *et al.* (2013) Structural characterization of cleaved, soluble HIV-1 envelope glycoprotein trimers. *J Virol* 87(17):9865-9872.
6. Klasse PJ, *et al.* (2013) Influences on trimerization and aggregation of soluble, cleaved HIV-1 SOSIP envelope glycoprotein. *J Virol* 87(17):9873-9885.
7. Sanders RW, *et al.* (2013) A next-generation cleaved, soluble HIV-1 Env Trimer, BG505 SOSIP.664 gp140, expresses multiple epitopes for broadly neutralizing but not non-neutralizing antibodies. *PLoS Pathog* 9(9):e1003618.
8. Julien JP, *et al.* (2013) Asymmetric recognition of the HIV-1 trimer by broadly neutralizing antibody PG9. *Proc Natl Acad Sci U S A* 110(11):4351-4356.
9. Ringe RP, *et al.* (2013) Cleavage strongly influences whether soluble HIV-1 envelope glycoprotein trimers adopt a native-like conformation. *Proc Natl Acad Sci U S A* 110(45):18256-18261.
10. Pugach P, *et al.* (2015) A native-like SOSIP.664 trimer based on an HIV-1 subtype B env gene. *J Virol* 89(6):3380-3395.
11. Wilkins MR, *et al.* (1999) Protein identification and analysis tools in the ExPASy server. *Methods Mol Biol* 112:531-552.
12. Voss NR, Yoshioka CK, Radermacher M, Potter CS, & Carragher B (2009) DoG Picker and TiltPicker: software tools to facilitate particle selection in single particle electron microscopy. *J Struct Biol* 166(2):205-213.
13. Lander GC, *et al.* (2009) Appion: an integrated, database-driven pipeline to facilitate EM image processing. *J Struct Biol* 166(1):95-102.
14. Ogura T, Iwasaki K, & Sato C (2003) Topology representing network enables highly accurate classification of protein images taken by cryo electron-microscope without masking. *J Struct Biol* 143(3):185-200.
15. Blattner C, *et al.* (2014) Structural delineation of a quaternary, cleavage-dependent epitope at the gp41-gp120 interface on intact HIV-1 Env trimers. *Immunity* 40(5):669-680.
16. McLellan JS, *et al.* (2011) Structure of HIV-1 gp120 V1/V2 domain with broadly neutralizing antibody PG9. *Nature* 480(7377):336-343.
17. Jardine J, *et al.* (2013) Rational HIV immunogen design to target specific germline B cell receptors. *Science* 340(6133):711-716.

18. Julien JP, *et al.* (2013) Broadly neutralizing antibody PGT121 allosterically modulates CD4 binding via recognition of the HIV-1 gp120 V3 base and multiple surrounding glycans. *PLoS Pathog* 9(5):e1003342.
19. Yasmeen A, *et al.* (2014) Differential binding of neutralizing and non-neutralizing antibodies to native-like soluble HIV-1 Env trimers, uncleaved Env proteins, and monomeric subunits. *Retrovirology* 11:41.
20. Bures R, *et al.* (2002) Regional clustering of shared neutralization determinants on primary isolates of clade C human immunodeficiency virus type 1 from South Africa. *J Virol* 76(5):2233-2244.
21. Li M, *et al.* (2006) Genetic and neutralization properties of subtype C human immunodeficiency virus type 1 molecular env clones from acute and early heterosexually acquired infections in Southern Africa. *J Virol* 80(23):11776-11790.
22. Seaman MS, *et al.* (2010) Tiered categorization of a diverse panel of HIV-1 Env pseudoviruses for assessment of neutralizing antibodies. *J Virol* 84(3):1439-1452.
23. Suloway C, *et al.* (2005) Automated molecular microscopy: the new Leginon system. *J Struct Biol* 151(1):41-60.
24. Li X, *et al.* (2013) Electron counting and beam-induced motion correction enable near-atomic-resolution single-particle cryo-EM. *Nat Methods* 10(6):584-590.
25. Mindell JA & Grigorieff N (2003) Accurate determination of local defocus and specimen tilt in electron microscopy. *J Struct Biol* 142(3):334-347.
26. Lyumkis D, *et al.* (2013) Cryo-EM structure of a fully glycosylated soluble cleaved HIV-1 envelope trimer. *Science* 342(6165):1484-1490.
27. Scheres SH (2012) RELION: implementation of a Bayesian approach to cryo-EM structure determination. *J Struct Biol* 180(3):519-530.
28. Chen S, *et al.* (2013) High-resolution noise substitution to measure overfitting and validate resolution in 3D structure determination by single particle electron cryomicroscopy. *Ultramicroscopy* 135:24-35.
29. Emsley P, Lohkamp B, Scott WG, & Cowtan K (2010) Features and development of Coot. *Acta Crystallogr D Biol Crystallogr* 66(Pt 4):486-501.
30. Larkin MA, *et al.* (2007) Clustal W and Clustal X version 2.0. *Bioinformatics* 23(21):2947-2948.
31. Huang J, *et al.* (2014) Broad and potent HIV-1 neutralization by a human antibody that binds the gp41-gp120 interface. *Nature* 515(7525):138-142.
32. Doria-Rose NA, *et al.* (2014) Developmental pathway for potent V1V2-directed HIV-neutralizing antibodies. *Nature* 509(7498):55-62.